

Laser sintering of dip-based all-copper interconnects

Luca Del Carro^{1,2}, Thomas Brunschwiler¹

¹IBM Research – Zurich
Säumerstrasse 4, 8830 Rüschlikon, Switzerland
ldc@zurich.ibm.com

²Complex Materials, Department of Materials
ETH Zürich
8093 Zürich, Switzerland

Martin Kossatz, Lucas Schnackenberg, Matthias Fettke

Pac Tech - Packaging Technologies GmbH
Am Schlangenhorst 7-9, 14641 Nauen, Germany

Ian Clark

Intrinsic Materials Ltd.
Farnborough, Hampshire GU14 0LX, United Kingdom

Abstract— The solder alloys applied in state-of-the-art flip-chip electrical interconnects are one of the main limits to improving the high power handling of this technology. To overcome this issue, the replacement of solder with interconnects purely made from copper is desirable, owing to copper's superior electromigration resistance with respect to solder. Recently, dip-based all-copper interconnects were shown to be a promising approach to form all-copper flip-chip interconnects by the sintering of Cu nano- and microparticles between copper pillars and pads. In this process, the Cu particles are applied on the pillar tips by a dip-transfer method and then collapsed onto pads, forming an assembly. Then, the assembly is sintered for 30 min in a thermal oven under constant flow of formic-acid-enriched nitrogen. After the sintering, copper joints that connect the pillars and pads are formed, resulting in the so called “dip-based all-copper interconnects”. Despite the large interest raised around this approach, the requirement of formic-acid application and the long sintering time limits its scalability. In our work, we report the first example of dip-based all-copper interconnects formed by laser sintering, without the application of formic acid and with a process time of only a few seconds. These results could lead to the development of a novel ultrafast and formic-acid free assembly technique of all-copper flip-chip interconnects.

Keywords— advanced flip-chip packaging; flip-chip electrical interconnects; all-copper interconnects; dip-based all-copper interconnects; laser sintering; copper nano-and microparticles; transient thermal finite element model

Advancement in flip-chip interconnect technology is constrained by the applied solder alloys, which have a limited power handling capability [1]. In this regard, interconnects made purely from copper are the designated candidates to replace the limited solder-based interconnects, with copper having superior electrical conductivity and

enhanced electromigration resistance with respect to solder [2][3].

Recently, *dip-based all-copper interconnects* have shown to be a promising approach to form copper-based interconnects by the sintering of copper nano- and microparticles between copper pillars and pads [4][5]. In this approach, the particles are applied onto the pillar tips of the chip by dip transfer and then collapsed onto the pads of the interposer, forming an assembly. After that, the particles are sintered by heating the formed assembly for 30 min in a thermal oven. During the sintering, the particles are constantly reduced by a flow of formic-acid-enriched nitrogen, and a maximum temperature of 200 °C is held for a dwell time of 5 min. After the sintering, porous copper joints that connect the pillars and pads are formed, creating the so called “*dip-based all-copper interconnects*”.

Furthermore, it was demonstrated that the porosity of the copper joints can be suppressed by application of bonding pressure during the sintering, leading to electrical resistivity comparable to bulk copper [6].

Despite these recent improvements, the requirements of a formic-acid atmosphere and the long sintering time demand the installation of dedicated flip-chip bonding systems with low throughput at high cost.

Lately, Zenou *et al.* reported the successful sintering of copper nanoparticles by direct laser irradiation in the millisecond time regime [7]. In this process, the sintering was achieved without the application of formic acid, despite obtaining an outstanding copper conductivity of 4x the bulk copper with a laser-pulse width (τ_p) of only 1 ms. The achievement was related to the addition of a reducing agent into the Cu paste formulation and to the faster kinetic of the process of laser sintering with respect to the reaction of Cu

oxidation. However, this study focused on the laser sintering of the copper nanoparticles via direct illumination, relevant for printed-electronics applications, but impractical for die bonding where a direct optical access to the copper nanoparticles is not available.

In our work, we explore the potential of laser sintering of copper nano- and microparticles by irradiation through the silicon substrate, for the formation of dip-based all-copper interconnects.

This rapid and localized heating technique has the potential to drastically reduce the required sintering time and avoid the application of formic acid during the process.

First, we report on the sintering of copper nano- and microparticles by indirect laser irradiation. Second, we apply this process to form dip-based all-copper interconnects.

I. MATERIALS & METHODS

A. Copper nano- and microparticles paste

In our work, a bi-modal paste containing a mixture of copper nano- and microparticles was used (Intrinsic IMC4106, Intrinsic Materials Ltd., Farnborough, UK). All nanoparticles were below 100 nm in size and the microparticles below 2 μm . All these particles were coated with a shell of organic binder and dispersed in a solvent. Moreover, a reducing agent was added to the formulation to reduce the native copper oxide present on the surface of the particles and partially prevent further oxide formation during the sintering process. The solid content of the paste was 86.7 wt %, which made it suitable for the dip transfer method (Table 1) [4].

Intrinsic IMC4106 could be sintered in a thermal oven at 230 $^{\circ}\text{C}$ without formic acid application, reporting a resistivity of 10x the one of bulk copper.

TABLE 1: COPPER PASTE FORMULATION

Paste name	Sintering temperature [$^{\circ}\text{C}$]	$P_{\text{sintered paste}}$ [$\mu\Omega\cdot\text{cm}$]	Metal load [wt %]
Intrinsic IMC4106	230	17	86.7

B. Test sample design and fabrication

For this study, mechanical test vehicles consisting of chip and substrate made of silicon were design and fabricated.

Silicon substrates of 10*10 mm^2 were prepared from <100> single side polished silicon wafers. Their front side (FS) was coated by sputtering with 10 nm of Ti and 100 nm of Cu.

Silicon chips of 8*8 mm^2 were made with a pillar array on the FS, which was fabricated by deep-reactive ion etching (RIE) in order to mimic the copper pillars used in flip-chip technology. The pillars were 50 μm in diameter and height, with a pitch distance of 110 μm . As for the silicon

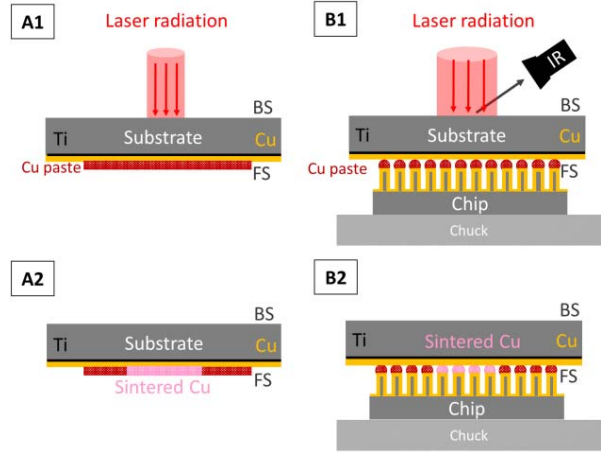


Figure 1: Schematic representation of the laser sintering procedure: A) laser sintering of copper nanoparticle film, B) laser sintering of dip-based all-copper interconnects. In both the experiments, the laser beam area is smaller than the area of the Cu-paste, resulting in a partial-area sintering. The back side (BS) and front side (FS) of the silicon substrate are labeled correspondingly. An infrared (IR) camera was used to record the temperature profile on the BS of the substrate during the sintering procedure B.

substrates, the FS of the chips was coated with 10 nm of Ti and 100 nm of Cu.

C. Laser apparatus & sintering procedure

A SB²-Jet laser system (Pac Tech, Nauen, Germany), equipped with a Nd:YAG laser ($\lambda=1064\text{nm}$, 100 W maximal optical output power) was used to study the copper nanoparticles sintering by indirect laser irradiation.

First, a 20 μm thick copper-paste film was doctor bladed onto the FS of the silicon substrate (Figure 1A). Then the laser was irradiated on the back side (BS) of the substrate in atmospheric conditions, projecting a Gaussian-shaped beam spot of 1 mm in diameter.

A similar laser system was used for the laser sintering of dip-based all-copper interconnects, with the maximal optical power increased to 200 W. The Cu particles were placed onto the pillars by dipping the silicon chip into a doctor-bladed-thin film of Cu paste, with a thickness of 20 μm . After the dipping, the chip was collapsed onto the substrate forming the assembly, which was then placed on the stainless steel chuck of the laser apparatus. Finally, the BS of the substrate was exposed to a laser beam of 2mm diameter in atmospheric conditions (Figure 1B). For some set of laser parameters, the temperature profile of the irradiated area of the substrate BS was recorded with an infrared (IR) camera.

In both the sintering procedures, the laser beam area was significantly smaller than the one coated with the Cu paste, resulting in a partial sinter of the area coated with the Cu

paste. This limitation was tolerated because the goal of our work was to explore the feasibility of the process of laser sintering. To this end, a customized set-up for laser bonding will be considered in future work.

TABLE 2 : THERMAL PROPERTIES OF THE ASSEMBLY, REPORTING THE THERMAL CONDUCTIVITY (κ), THE HEAT CAPACITY (C_p), THE DENSITY AND THE THICKNESS OF THE BODIES (T) USED IN THE TRANSIENT THERMAL MODEL.

Body	Material	κ [W/m*K]	C_p [J/Kg*K]	Density [Kg/m ³]	T [μ m]
Substrate	Silicon	148	712	2330	525
Interconnects	Interconnects layer	78	385	1758	50
Chip	Silicon	148	712	2330	525

D. Characterization techniques

The morphology of the sintered Cu was characterized as a function of the applied laser pulse width (τ_p) by optical microscopy (Leica DVM2500) and scanning electron microscopy (SEM, V400ACE, FEI, USA), exposing cross-sections of the sintered layers by focus ion beam (FIB, V400ACE, FEI, USA). The porosity percentage of the sintered Cu was derived by post-processing of the recorded top-view SEM images (Image J). The resistivity of the sintered Cu film was measured by a 4-point contact probe (Jandel universal probe stand).

Cross sections of the formed interconnects were prepared by polishing (Struers Tegramin 20, Denmark) and ion milling (Oxford Instruments, Ionfab 300, UK) and imaged with SEM. Moreover, the shear strength of the interconnects was assessed by shear testing the sintered assembly. In this test, the chips were sheared off from the substrates in a displacement-controlled experiment with a rate of 1 μ m/s using a SELmaxi load frame (Thelkin AG, Winterthur, Switzerland). The force of shearing obtained was divided by the effective sintered area, to obtain the average shear strength of a single interconnect. The results were averaged over 5 sample per given set of sintering parameters.

For some experiments, the temperature profile on the substrate BS was recorded with an IR camera (CT 3M1, Optris), during the laser irradiation. The response time of the camera was 1 ms and the set range of temperature spaced from 150 $^{\circ}$ C to 1800 $^{\circ}$ C.

E. Transient-thermal model

In this work, a transient thermal 3D finite elements model was established in ANSYS Workbench to simulate the resulting thermal profile upon laser irradiation of the

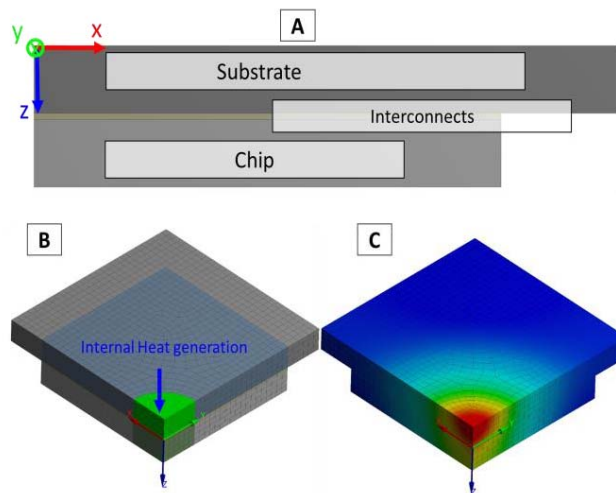


Figure 2: Schematic representation of the modeled geometry of the assembly. A) Cross-section view of the assembly that shows the three main bodies: the substrate, the interconnects and the chip, B) Isometric view of the assembly underling the body section where the condition of internal heat generation is imposed, C) Isometric view of the resulting thermal gradient at a given time during the laser irradiation.

assembly formed by: the substrate, the interconnects and the chip. The geometry of the assembly is shown in Figure 2. Due to symmetry reasons, only a quarter of the real assembly needed to be modeled. Furthermore, temperature invariant material properties were assumed (Table 2). The properties of the interconnects layer were calculated assuming 35% of the volume to be occupied by copper and the remaining 65% by air, as a result of the structuring of the chip FS with the pillars array.

The initial temperature of the bodies was set to be 20 $^{\circ}$ C. Natural convection with a heat transfer coefficient (h) of 7 W/m²*K was applied to the BS surface of the substrate to represent the heat transfer to the environment by natural convection. A boundary condition with h of 3000 W/m²*K was applied to the unstructured surface of the chip, to simulate the thermal contact with the stainless steel chuck. This h value was derived by comparing the simulation with the experimental profile until find an optimal accordance.

The thermal effect of the laser irradiation was simulated by establishing internal heat generation in the part of the substrate directly irradiated by the beam. Being the material properties temperature independent, the temperature response of the model scaled linearly with the input power. Therefore, the model was performed with a nominal input power of 100 W, to later scale it to all the experimental power inputs to model.

From the experiments, only the values of the irradiated laser power were known, due to the uncertainty in the optical properties of the used materials and consequently in the quantity of energy absorbed by the material upon irradiation. For this reason, the thermal profile resulting from the simulation was scaled to the input values of laser

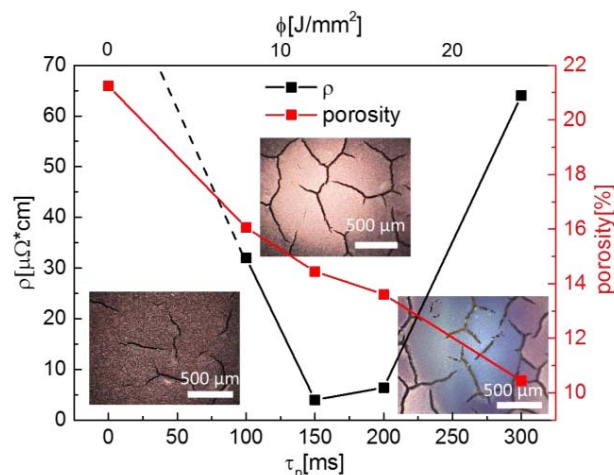


Figure 3: Resistivity and residual porosity of the sintered Cu reported as a function of the laser pulse width (τ_p) and laser fluence (ϕ). The dashed line leads to the resistivity value of $10 \mu\Omega\cdot\text{cm}$ of the non-sintered Cu paste. Inset: bright-field optical images of the laser-processed Cu film for a τ_p of (from left to right) 0, 150 and 300 ms, respectively.

power and then corrected by a factor $\eta = 0.92$ calculated analytically, matching the experimental profiles with the simulations, in order to keep the mismatch in the maximum-temperature value below 4.5 %.

II. RESULTS AND DISCUSSION

A. Laser sintering of copper nano- and microparticles

The effects of the input-laser irradiation on the sintering of the Cu nano- and microparticles were evaluated keeping the laser irradiance constant at 79 W/mm^2 , while τ_p was varied from 2 to 300 ms.

The results of the τ_p variation on the electrical resistivity (ρ) and residual porosity of the sintered Cu film were reported in Figure 3. Initially, the increase in τ_p resulted in a reduction of the ρ , reaching a minimum of $4 \mu\Omega\cdot\text{cm}$ for 150 ms. For larger τ_p values, the ρ increased, rising to $64 \mu\Omega\cdot\text{cm}$ for 300 ms. The increment of the τ_p resulted in a reduction of residual porosity of the sintered Cu. The porosity decreased from an initial 21%, which is obtained without any laser irradiation through complete evaporation of the solvent at $70 \text{ }^\circ\text{C}$, down to 14% for τ_p of 150 ms. By further increasing the pulse width, a reduction of the porosity to 10% was observed.

Moreover, bright-field microscope images of the Cu film are reported in Figure 3, showing a sharp color change of the laser-processed Cu film as a function of τ_p . The color changed from an initial brown, typical of non-sintered Cu paste, to pink for the samples irradiated with a pulse duration of 150 ms. For higher τ_p , a discoloration of the sintered Cu to blue was observed. Furthermore, the

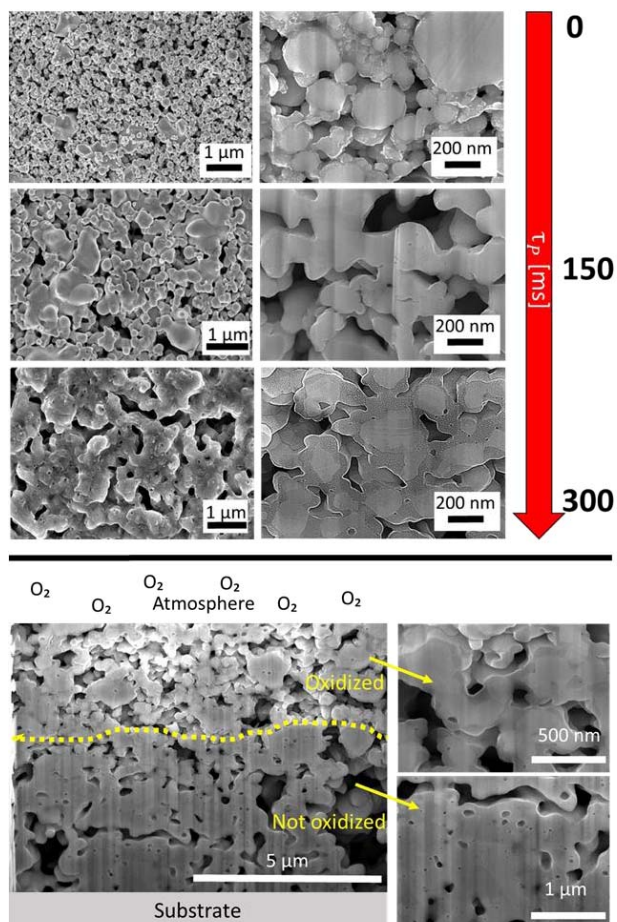


Figure 4: TOP: top-view (left column) and cross section (right column) SEM images of the Cu film sintered by indirect laser irradiation as a function of τ_p . BOTTOM: cross-section SEM images showing the partial extension of the copper oxide layer from the surface of the Cu film exposed to the atmosphere.

formation of large cracks in all the sintered Cu film was detected.

The morphology of the sintered Cu was strongly affected by τ_p (Figure 4). Extensive necking and material densification was observed in the samples irradiated for 150 ms with respect to the non-irradiated ones. In addition, the growth of a copper oxide layer of $60 \pm 10 \text{ nm}$ was observed around the Cu grains for τ_p of 300 ms. The extension of the oxidized Cu was limited to a depth of $3 \mu\text{m}$ from the surface of the film exposed to the atmosphere.

These results show that the Cu nano- and microparticles can be successfully sintered by indirect laser irradiation without the utilization of formic acid, obtaining in 150 ms a sintered film with a resistivity of only 4x the bulk Cu.

In this process, the laser energy is expected to be absorbed exclusively by the substrate, due to the opacity of the

sputtered Ti and Cu coatings to the input radiation [8]. The applied τ_p is long compared to the picoseconds time domain of the electron-phonon thermalization, suggesting a complete dissipation of the absorbed energy in heat [9][10]. After that, the generated heat diffuses from the substrate to the Cu-paste layer, where it activates the reducing agent that removes the native copper oxide from the surface of the particles, initiating the sintering process.

The amount of heat generated increases with the extension of τ_p . A deficit in the amount of heat generated leads to an insufficient energy transfer to the Cu film and consequently to the particles not sintering.

On the other hand, an excess in the heat generation causes overheating of the Cu film, provoking the oxidation of the first few microns from the surface exposed to the atmosphere. This limited extension from the surface suggests that the oxygen present in the atmosphere can diffuse only through the first few microns of the Cu film before the cool down, which inhibits further oxidation reaction.

The described relationship between the amount of heat generated and the sintering process explains the reported trends in ρ and residual porosity of the laser-processed Cu as a function of τ_p . The ρ decreases until an optimum amount of heat is generated, and increases later when the oxidation reaction takes place. The residual porosity initially decreased due to the densification related to the sintering of the particles, to then further drop due to the volumetric expansions caused by the copper oxidation [11].

The observed color change of the laser-processed Cu film is related to the alteration of the reflectivity as a function of the thickness of the copper oxide layer [12]. Moreover, the detected cracks formed in all the sintered films can be associated to the solvent evaporation and consequent shrinkage of the thin film. Zürcher *et al.* demonstrated that the mixture of nano- and microparticles prevents the formation of these large cracks in dip-based all-copper interconnects [4].

The study of the sintering of Cu nano- and microparticles by indirect laser irradiation is used as a starting point for the application of this technique to form dip-based all-copper interconnects. In fact, the discussed results on the color, morphology and resistivity changes of the laser-processed Cu particles are used in the following section as reference to estimate the performance of the less accessible interconnects after laser irradiation.

B. Laser sintering of dip-based all-copper interconnects

The formation of dip-based all-copper interconnects by laser sintering was explored by systematically varying the laser irradiance and τ_p from 7 to 33 W/mm² and from 100 to 5000 ms, respectively (Figure 5).

From this parametric study, three regimes were identified as a function of the applied laser fluence (ϕ): 1) a non-sintering

regime for ϕ values below 26 J/mm², where the Cu paste did not sinter and exhibited the typical brown color, 2) a sintering regime in the range of 26 J/mm² < ϕ < 44 J/mm², where a successful bonding was obtained resulting in pink sintered Cu, and 3) an oxidation regime for ϕ above 44 J/mm², where discoloration of the Cu particles and oxide growth were observed. In the sintering regime, the τ_p could be reduced from 3 to 1.5 s by increasing the laser irradiance from 10 to 26 W/mm², always resulting in a successful bond. Furthermore, glowing of the illuminated area of substrate BS was observed during the laser pulse for irradiances above 20 W/mm². However, this phenomenon didn't lead to visible damage of the irradiated surface.

Cross-section images of dip-based all-copper interconnects formed with ϕ of 35 J/mm² showed an effective bonding between the pillars and pads, held by the sintered Cu joints

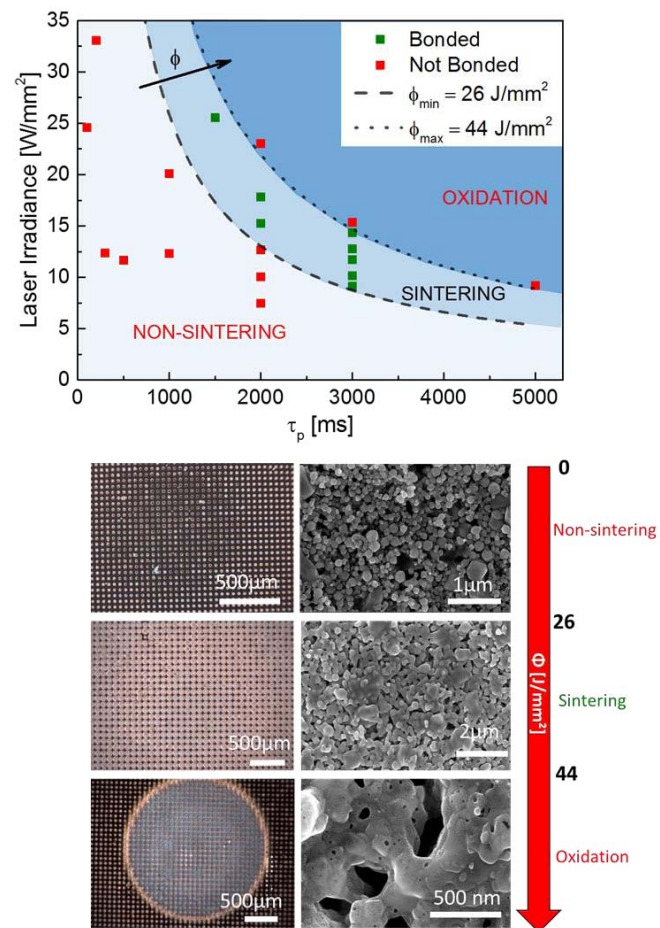


Figure 5: TOP: Sintering map of the tested laser parameters reported as laser irradiance vs τ_p . The final condition of the assembly is color labeled. Isoenergy lines are reported, resulting in the division of the map into 3 regimes: non-sintering, sintering and oxidation. BOTTOM: bright-field optical images (left column) and SEM images (right column) of samples processed in the three regimes.

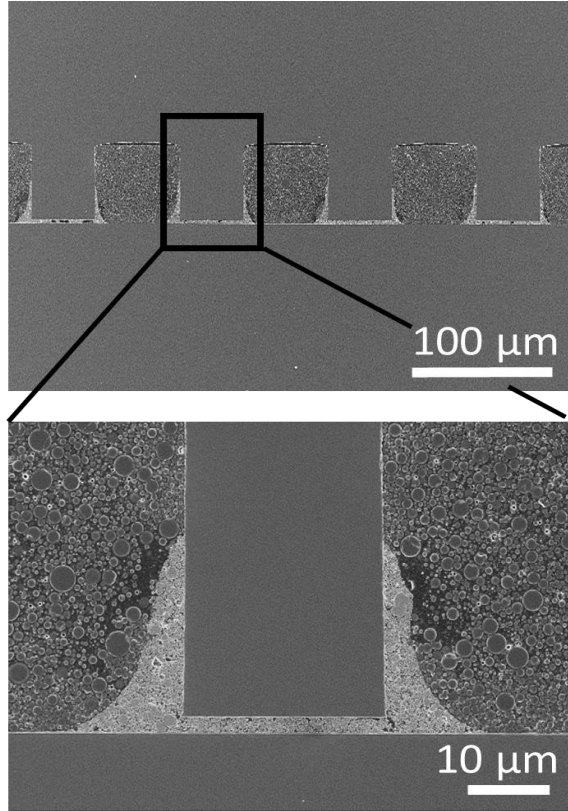


Figure 6: Cross-section SEM images of a sample processed for 3 s with 11.6 W/mm².

(Figure 6). Moreover, a good interdiffusion between the sintered and sputtered Cu layers was observed with few voids formed in the Cu joints. An average shear strength of 20 ± 3 MPa was measured for the samples processed at ϕ between 35 and 38 J/mm².

For some of the tested sets of input-laser parameters, the maximum temperature (T_{MAX}) reached on the BS of the substrate was recorded (Figure 7). The highest T_{MAX} value of 791 °C was measured for the samples irradiated with 33 W/mm² for 200 ms. A decrease in the applied laser irradiance resulted in a monotonic reduction of the T_{MAX} , with the recorded temperature always below 400 °C for laser irradiances under 18 W/mm². Within the sintering regime, a decrease of the measured T_{MAX} from 590 to 245 °C was obtained decreasing the laser irradiance from 26 to 10 W/mm².

The established transient thermal model was used to predict the resulting T_{MAX} on the BS of the substrate for fixed ϕ of 26 and 44 J/mm² (Figure 7), which were previously identified as the lower and upper boundaries of the sintering regime. A good agreement between the model and the experimental data was obtained for temperatures below 400 °C, with a maximal error of 4.5% in the prediction. However, for higher temperatures the predictions deviate

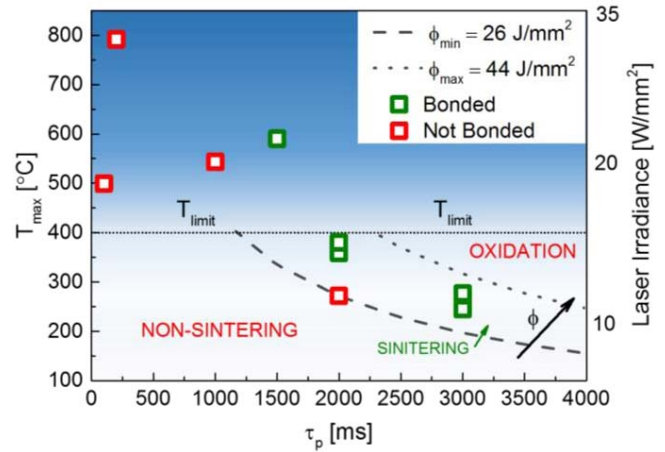


Figure 7: Map of the recorded maximum temperature (T_{MAX}) on the substrate BS reported as a function of τ_p . Values of the applied laser irradiance are displayed. The final condition of the assembly is color labeled. Isoenergy lines derived by the established transient thermal model are shown for T_{MAX} below 400 °C, resulting in the segmentation of the map in 3 regimes: non-sintering, sintering and oxidation.

substantially from the experimental measurements, with a maximal error above 10%.

Furthermore, the T_{MAX} distribution along the x and z axes of

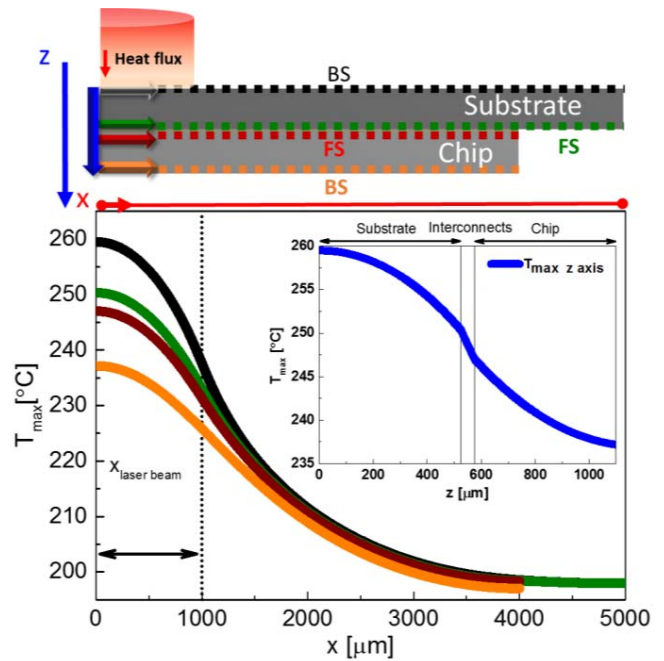


Figure 8: Simulated distribution of the maximal temperature (T_{MAX}) along the x axis of all the interfaces of the assembly. The considered interfaces are color labeled in the schematic representation of the assembly (TOP). Inset: simulated T_{MAX} distribution along the z axis situated at the center of the assembly. The spatial division between the different bodies of the assembly is marked.

all the interfaces of the assembly was simulated for a successful bonding test performed in 3 s by application of 11.6 W/mm^2 (Figure 8). Due to the small area of the laser beam with respect to the assembly one, a decrease in T_{MAX} along the x axis at all the interfaces was predicted. Along the x axis of the substrate FS (green curve in Figure 8), where the Cu particles were applied, the T_{MAX} dropped 6.8% within 1 mm from the hottest point in the origin, losing a total 21% along the 5 mm of the substrate. Along the z axis, a small drop of 3.5% in T_{MAX} was predicted from the irradiated BS of the substrate to the FS.

The results show that dip-based all-copper interconnects can be successfully formed by laser sintering without the application of formic acid, just simply exposing the assembly to maximal temperatures below $400 \text{ }^\circ\text{C}$ for only a few seconds.

To form a stable bond, the assembly has to be irradiated with an optimal range of ϕ , which thermally activates the sintering of the Cu particles without leading to overheating of the sintered Cu and consequent growth of Cu oxide. To this end, the relationship between the generated T_{MAX} and the process time is crucial: 1) the high temperature has to be held long enough to allow the sintering of the Cu particles, and 2) by increasing the value of T_{MAX} it is possible to decrease the process time. However, a limit in the allowed T_{MAX} has to be set to avoid damage in the back-end of the line (BEOL) and in the active components of the chip. In this work we set the bonding-temperature limit to $400 \text{ }^\circ\text{C}$, which is safe for CMOS technology [13].

The presented model doesn't match the experimental measurements of T_{MAX} for values above $400 \text{ }^\circ\text{C}$, due to the glowing of the substrate BS observed during irradiation. In fact, the emission of radiation causes a change in the optical properties of the silicon and consequently affects the absorption of the input radiation non linearly [14]. Nevertheless, all the values of input laser irradiance used in this work are far from the damage threshold of silicon, which was found by Wang *et al.* to be 1400 W/mm^2 for a laser wavelength of 1064 nm and τ_p of 2 ms [15].

The small drop in temperature predicted along the z axis, from the substrate BS to the interconnects, indicates a high efficiency in local heating offered by the laser sintering process. On the other hand, the large temperature loss estimated along the x axis underlines the limit of the laser apparatus used, which cannot homogeneously heat the assembly area due to the smaller spot size.

The reported cross-section images and the measured shear strength values are comparable to the ones obtained for dip-based all-copper interconnects sintered in a thermal oven without the application of bonding pressure [6]. Moreover, the pink color of the sintered Cu observed for samples processed in the sintering regime suggests an electrical resistivity of the Cu joint in the order of $10 \mu\Omega\cdot\text{cm}$.

III. CONCLUSION

In this work, we explored the laser sintering of copper nano- and microparticles by irradiation through the silicon substrate to form dip-based all-copper interconnects.

First, it was demonstrated that Cu nano- and microparticles can be successfully sintered by laser irradiation through the substrate, without utilization of formic acid. Within only 150 ms, a sintered Cu film with the electrical resistivity of 4x the bulk Cu was obtained. Furthermore, the porosity, the morphology and the color of the laser-processed Cu film were evaluated from the not sintered to the oxidized state. From this characterization, the purely thermal nature of the sintering process triggered by the laser irradiation was demonstrated. Moreover, the characterization of the laser-processed Cu film resulted in a useful reference to evaluate the final status of the less accessible interconnects formed by laser sintering.

Second, we presented the first example of dip-based all-copper interconnects formed by laser sintering. These interconnects were accomplished without the application of formic acid, reaching temperatures below $400 \text{ }^\circ\text{C}$ for only a few seconds. The optimum ϕ regime to bond the used assembly was found to be between 26 and 44 J/mm^2 . The resulting T_{MAX} on the substrate BS was measured and its role in the bonding analyzed, concluding that 1) the high temperature has to be held long enough to allow the sintering of the Cu particles, and 2) by increasing the value of T_{MAX} it is possible to decrease the process time. Furthermore, a transient thermal model able to predict the T_{MAX} for values below $400 \text{ }^\circ\text{C}$ was established. In addition, the characterization of the formed interconnects showed mechanical properties comparable to state-of-the-art dip-based all-copper interconnects.

In conclusion, this work demonstrates the feasibility of fabricating dip-based all-copper interconnects by laser sintering, which can lead to the development of a novel ultrafast and formic-acid free assembly technique of all-copper flip-chip interconnects.

IV. OUTLOOK

We consider to use a laser-apparatus with a beam area comparable to the one to sinter will be used to form dip-based all-copper interconnects across the entire chip. Moreover, bonding pressure will be applied during the irradiation to improve the electrical and mechanical performances of the interconnects.

The evaluation of dip-based all-copper interconnects formed by laser sintering will be extended to the bonding of die on organic laminate, where the large thermal expansion mismatch is an issue for the application of dip-based all-copper interconnects sintered in a thermal oven.

ACKNOWLEDGMENT

The authors thank Thomas Wildsmith, previously at Intrinsic Materials Ltd., for his help in the early stages of the work, Ute Drechsler and all the other members of the Binning and Rohrer Nanotechnology Center (BRNC) for their help in the fabrication of the test vehicles, Dr. Bruno Michel, Prof. André R. Studart and Dr. Walter Riess for their continuous support.

This project has been supported by the Swiss National Foundation, Project 200021_160189: “Controlled Drying of Colloidal Suspensions in Porous Structures for Neck-Based Interconnects.”

REFERENCES

- [1] R. Ghaffarian, “Microelectronics packaging technology roadmaps, assembly reliability, and prognostics,” *Facta universitatis - series: Electronics and Energetics*, vol. 29, no. 4, pp. 543–611, 2016.
- [2] M. Lu, “Effect of microstructure and alloy doping on electromigration in Pb-free solder interconnect,” *IEEE International Integrated Reliability Workshop Final Report*, pp. 190–196, 2013.
- [3] Y. S. Lai, Y. T. Chiu, and J. Chen, “Electromigration reliability and morphologies of cu pillar flip-chip solder joints with cu substrate pad metallization,” *Journal of Electronic Materials*, vol. 37, no. 10, pp. 1624–1630, 2008.
- [4] J. Zurcher, L. Del Carro, G. Schlottig, D. N. Wright, A. S. B. Vardoy, M. M. V. Taklo, T. Mills, U. Zschenderlein, B. Wunderle, and T. Brunchwiler, “All-Copper Flip Chip Interconnects by Pressureless and Low Temperature Nanoparticle Sintering,” *Proceedings - Electronic Components and Technology Conference*, vol. 2016–August, pp. 343–349, 2016.
- [5] T. Brunchwiler, G. Schlottig, A. Sridhar, A. La Porta, O. Ozsun, J. Zurcher, R. Strassle, L. Del Carro, and P. A. M. Bezerra, “Scalable packaging platform supporting high-performance 3D chip stacks,” *2017 Pan Pacific Microelectronics Symposium, Pan Pacific 2017*, 2017.
- [6] L. Del Carro, J. Zuercher, S. Gerke, T. Wildsmith, G. Ramos, and T. Brunchwiler, “Morphology of Low-Temperature All-Copper Interconnects Formed by Dip Transfer,” in *2017 IEEE 67th Electronic Components and Technology Conference (ECTC)*, 2017, pp. 961–967.
- [7] M. Zenou, O. Ermak, A. Saar, and Z. Kotler, “Laser sintering of copper nanoparticles,” *Journal of Physics D: Applied Physics*, vol. 47, no. 2, p. 25501, 2014.
- [8] M. A. Ordal, L. L. Long, R. J. Bell, S. E. Bell, R. R. Bell, R. W. Alexander, and C. A. Ward, “Optical properties of the metals Al, Co, Cu, Au, Fe, Pb, Ni, Pd, Pt, Ag, Ti, and W in the infrared and far infrared,” *Applied Optics*, vol. 22, no. 7, p. 1099, 1983.
- [9] H. E. Elsayed-Ali, T. B. Norris, M. A. Pessot, and G. A. Mourou, “Time-resolved observation of electron-phonon relaxation in copper,” *Physical Review Letters*, vol. 58, no. 12, pp. 1212–1215, 1987.
- [10] J. R. Goldman and J. A. Prybyla, “Ultrafast dynamics of laser-excited electron distributions in silicon,” *Physical Review Letters*, vol. 72, no. 9, pp. 1364–1367, 1994.
- [11] M. Yin, C.-K. Wu, Y. Lou, C. Burda, J. T. Koberstein, Y. Zhu, and S. O’Brien, “Copper Oxide Nanocrystals,” *Journal of the American Chemical Society*, vol. 127, no. 26, pp. 9506–9511, 2005.
- [12] M. Zenou, O. Ermak, A. Saar, and Z. Kotler, “Laser sintering of copper nanoparticles,” *Journal of Physics D: Applied Physics*, vol. 47, no. 2, p. 25501, 2014.
- [13] P. Batude, M. Vinet, A. Pouydebasque, C. Le Royer, B. Previtali, C. Tabone, J. M. Hartmann, L. Sanchez, L. Baud, V. Carron, A. Toffoli, F. Allain, V. Mazzocchi, D. Lafond, O. Thomas, O. Cueto, N. Bouzaida, D. Fleury, A. Amara, S. Deleonibus, and O. Faynot, “Advances in 3D CMOS sequential integration,” *Technical Digest - International Electron Devices Meeting, IEDM*, no. 110, pp. 345–348, 2009.
- [14] H. Rogne, P. J. Timans, H. Ahmed, H. Rogne, P. J. Timans, and H. Ahmed, “Infrared absorption in silicon at elevated temperatures Infrared absorption in silicon at elevated temperatures,” vol. 2190, no. 1996, pp. 21–24, 2016.
- [15] X. Wang, D. H. Zhu, Z. H. Shen, J. Lu, and X. W. Ni, “Surface damage morphology investigations of silicon under millisecond laser irradiation,” *Applied Surface Science*, vol. 257, no. 5, pp. 1583–1588, 2010.